Article

Dietary lipids are largely deposited in skin and rapidly affect insulating properties

Nick Riley[1], Ildiko Kasza[1], Isabel D. K. Hermsmeyer [2], Michaela E. Trautman[3,4], Greg Barrett-Wilt[5], Raghav Jain [6], Judith A. Simcox [6,7], Chi-Liang E. Yen[8], Ormond A. MacDougald [2], Dudley W. Lamming [3,4] & Caroline M. Alexander [1] ✉

Skin is a regulatory hub for energy expenditure and metabolism, and alteration of lipid metabolism enzymes in skin impacts thermogenesis and obesogenesis in mice. Here we show that thermal properties of skin are highly reactive to diet: within three days, a high fat diet reduces heat transfer through skin. In contrast, a dietary manipulation that prevents obesity accelerates energy loss through skins. We find that skin is the largest target for dietary fat delivery, and that dietary triglyceride is assimilated by epidermis and dermal white adipose tissue, persisting for weeks after feeding. With caloric-restriction, mouse skins thin and assimilation of circulating lipids decreases. Using multi-modal lipid profiling, keratinocytes and sebocytes are implicated in lipid changes, which correlate with thermal function. We propose that skin should be routinely included in physiological studies of lipid metabolism, given the size of the skin lipid reservoir and its adaptable functionality.

A growing body of research highlights the influence of altered skin function on system-wide metabolism and energy expenditure. Mice with gene mutations that specifically affect the lipid composition of their skin exhibit changes in thermoregulation, resistance to diet-induced obesity, and enhanced insulin sensitivity[1,2]. As one example, mice with a keratinocyte-specific mutation of the lipid transport protein, acyl-CoA-binding protein (ACBP), show impaired thermal barrier function (increased TEWL), increased energy expenditure and food intake, altered lipid metabolism in liver, increased lipolytic flux in white adipose tissue (WAT), iWAT beiging, and resistance to diet-induced obesity. These systemic changes of energy homeostasis are reversed by housing mice at thermoneutrality or inhibiting thermogenic β-adrenergic signaling[3,4]. Other examples of epidermal regulation of energy homeostasis include genetic studies of ACER1, DGATs, ELOVL and SCD enzymes, discussed in detail by us and others[2,5–9]. These studies conclude that the rate of heat loss through skin determines the rate of heat production required to maintain body temperature, which in turn regulates energy homeostasis, to determine the overall metabolic strategy.

However, the mechanisms underlying the regulation of the skin thermal barrier are not known, and this presents a significant translational knowledge gap, as the manipulation of skin properties may offer a valuable approach for improving health. Indeed, heat transfer properties across skin are so fundamentally integrated with health and frailty that thermal (FLIR) facial images can be used to measure human age (± 5 years) and diagnose aspects of metabolic health[10]. The heat transfer properties of skin are difficult to mathematically predict a priori[11], most notably because this tissue is so dynamic, with changing blood flow and liquid transpiration.

Skin is comprised of at least three, closely-apposed lipid-enriched layers: these are the pelt (hair), with associated waxy sebome, the stratum corneum, assembled by epidermal keratinocytes, and a skin-associated adipose depot, the dermal white adipose tissue (dWAT), with unique function and regulation[5,12]. The properties of any of the

[1]McArdle Laboratory for Cancer Research, University of Wisconsin-Madison, Madison, USA. [2]Department of Molecular & Integrative Physiology, University of Michigan, Michigan, USA. [3]Department of Medicine, University of Wisconsin-Madison, Madison, USA. [4]William S. Middleton Memorial Veterans Hospital, Madison, USA. [5]Biochemistry Mass Spectrometry Core, Madison, USA. [6]Department of Biochemistry, University of Wisconsin-Madison, Madison, USA. [7]Howard Hughes Medical Institute, University of Wisconsin-Madison, Madison, USA. [8]Department of Nutritional Sciences, University of Wisconsin-Madison, Madison, USA. ✉e-mail: cmalexander@wisc.edu

three biomaterials could therefore be important effectors of energy expenditure.

In this study, we test whether total skin function is an early responder to conditions that change metabolism, and if so, which of the cell types and thermal components correlate with functional changes. We focus on the molecular lipidome, for two reasons. The first is the body of experimental data demonstrating that mutations of epidermal lipid metabolic enzymes confer changes of system-wide metabolism, and the second is that lipid composition is known to be modified by environmental temperature changes throughout the biological phyla, suggesting that altered lipid biosynthesis is an ancient means of temperature-induced adaptation[13].

Using a short timeline of 3 days, we find that skins become more insulating in response to an obesogenic high fat diet. Indeed, we find the major site of delivery for dietary fats is mouse skin, and delivery is ablated if mice are calorie-restricted. Vice versa, we find that skins become more heat-permeable in response to a diet low in the branched chain amino acid, isoleucine, which is a diet that promotes leanness, health and longevity. Overall, we conclude that skin properties are highly modifiable, and amongst the earliest functional responders to diets that affect obesogenesis and energy expenditure. Using multimodal lipidomic analysis, we show that the amount and specifics of the lipids from sebome and epidermis change in parallel with functional changes, suggesting that both sebocyte and keratinocyte could be manipulated to promote heat flux through skins.

Results

Skin is an early responder to a change of diet

Most studies of metabolic adaptation to diet or environment use a minimum 2, 3 weeks after the diet switch before testing for phenotypic alterations associated with energy expenditure. Our goal was to

evaluate whether skin adaptation preceded or followed other significant changes, such as an increased body weight in response to high fat feeding. We therefore chose 3 days after the dietary switch to a high fat diet (**HFD**; 60% calories from fat, provided as 90% lard, 10% soybean oil, compared to control diet 18% calories from fat, provided as soybean oil) for subsequent analyses.

Both male and female BALB/cJ mice ate more kilocalories (Kcal) per day when switched to HFD (Fig. 1A); however, after 3 days, these mice did not yet show a significant change of body weight (Fig. 1B). The average area of perigonadal white adipocytes and dermal white adipocytes was also unchanged and there were no significant changes of skin morphology, including dWAT thickness (Supplementary Fig. 1).

To assess the effect of HFD on the thermal properties of skins, we used several techniques. Assay of trans-epidermal water loss (**TEWL**) indicates the rate of evaporative cooling, which we have previously shown is a major effector of energy loss for mice[6]; this is "insensible" water loss at environmental temperatures below body temperature, thus not associated with the heat loss mechanisms activated when body temperature is too high, or the mouse is stressed (such as superficial blood vessel dilation). The assay is done ex vivo on a warm, wet heat block, to eliminate effects attributable to changing blood flow, and TEWL is reported for shaved skin (dorsal "**skin**") and **pelt** (unshaved), as described previously[6]. Heat transfer across HFD-fed mouse skin and pelt was significantly reduced, especially for males (Fig. 1C, D). Surface thermography using a forward-looking, infrared camera (**FLIR**) was used to assess radiative heat losses and skin insulation properties. The lower surface temperature of pelts and skins from HFD-fed mice, compared to the heat block background, reflects an increase in "insulation" (Fig. 1E). To corroborate results from BALB/cJ mice, we evaluated both male and female C57BL/6J mice and found that heat loss across skins and pelts was similarly reduced within 3 days
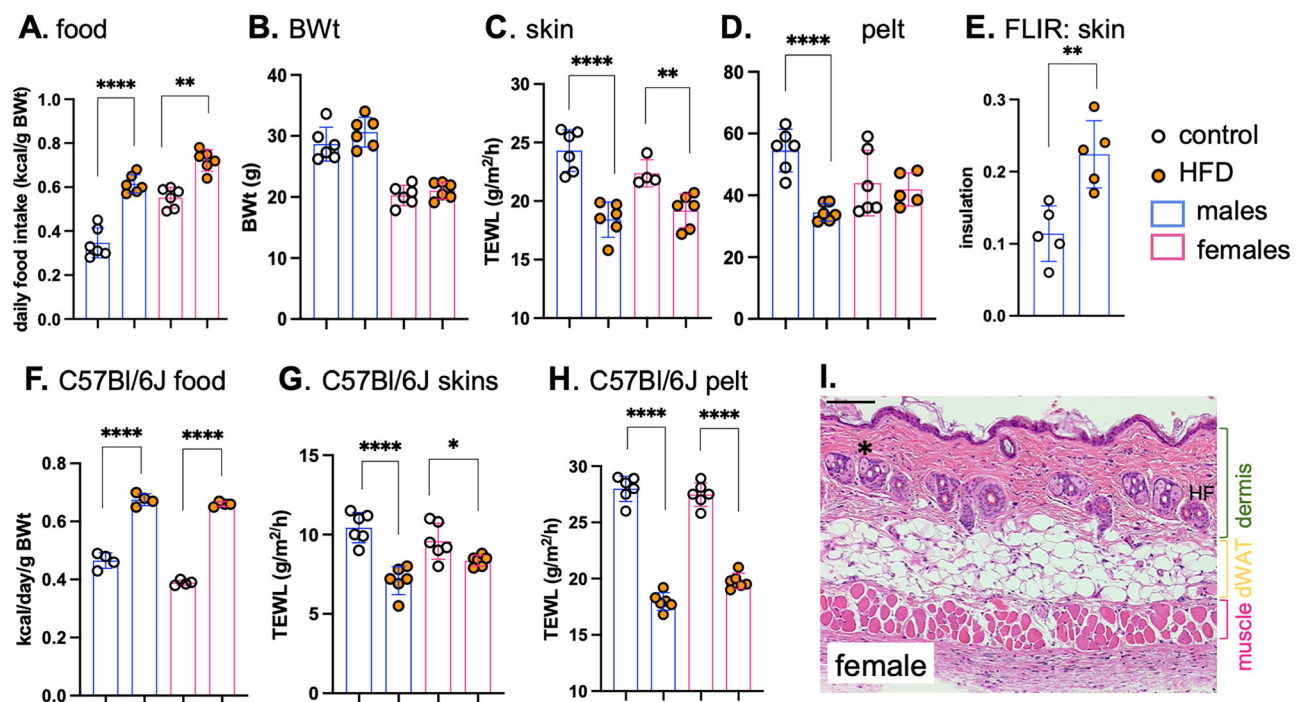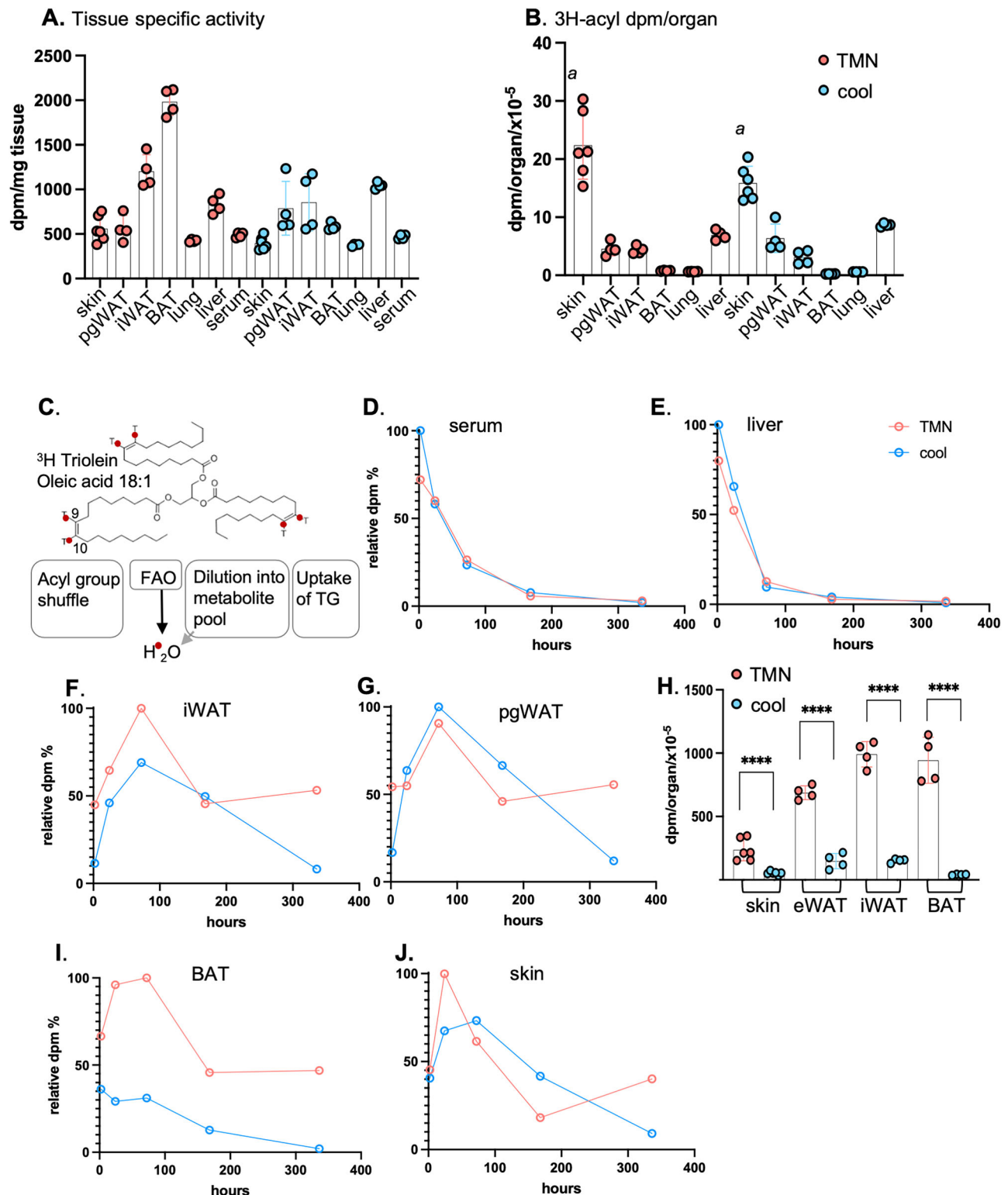

Fig. 1 | High fat diet consumption rapidly results in lower heat loss through skins. Male and female BALBc/J mice (10–15 weeks old) were switched to HFD for 3 days, and daily food consumption assessed together with their body weight (BWt; $n = 6$; **A**, **B**). **C** *Skin thermal properties* were measured by TEWL assay of skin (**C**) and pelt (**D**; $n = 4$–6), and by FLIR assay, where insulation is described as the difference in temperature between the top of the skin, and the adjacent heat block (**E**; measured in ^{0}C; $n = 5$). **F**–**H** *C57Bl/6J mice.* Male and female C57BL/6J mice were fed HFD for 3 days and assayed for their relative food consumption (**F**; $n = 3, 4$), and

the properties of their skins (assayed by TEWL of skin and pelt; **G**, **H**; $n = 6$). Data are presented as mean values +/− SD per mouse, and statistics calculated from 2-sided t-tests; *$p < 0.05$; **$p < 0.01$, ***$p < 0.001$, ****$p < 0.0001$. Specific p values are presented in Source Data files. **I** *Structure of skin biomaterial.* A representative H&E-stained section of female BALB/cJ skin annotated with the labels used for subsequent studies. (Supplementary Fig. 1 shows representative H&E-stained sections from both male and female BALB/c and C57BL/6J mice, fed HFD or not). Scale bar = 100 μm. Source data are provided as a Source Data file.

A. Tissue specific activity

B. 3H-acyl dpm/organ

C.

D. serum

E. liver

F. iWAT

G. pgWAT

H.

I. BAT

J. skin

of HFD feeding (Fig. 1F-H). A comparison of results from TEWL, FLIR and a thermistor-based heat transfer assay is shown in Supplementary Fig. 11, and the structure of the male and female mouse skin biomaterials under test is shown in Fig. 1I and **S1**.

A large fraction of dietary lipid is taken up by and stored in skin

At least two possibilities could explain a rapid response of skin to diet: the first is that high fat consumption sends an indirect cue to skin, and the second is that incorporation of dietary fats into skins changes thermal properties. To address these possibilities, we first tested

whether lipids could be delivered directly to skin from high fat diet. We administered a triglyceride radiotracer, 3H-[9,10] triolein, by gavage as described by Bartelt et al.[14] and assessed the assimilation of radiotracer in various tissues over the course of 2 weeks (serum, liver, BAT, iWAT, pgWAT and skin (Fig. 2, Supplementary Fig. 2). Triolein has different metabolic fates (Fig. 2C), including lipase-induced shuffle of oleate acyl chains to new triglycerides, or fatty acid oxidation stimulated by thermogenic activation at sub-thermoneutral housing temperatures. To characterize the changes of acyl flux due to thermogenesis, we compared tissue-specific dpm for BALB/cJ males and

Fig. 2 | Skins assimilate more dietary acyl lipid than any other organ and dietary fat persists in skin and adipose depots for several weeks. BALBc/J female mice (10–15 weeks old) were administered 3H-triolein by gavage and assessed 24 h later (**24 h post-gavage, pg**) for incorporation of radiolabel into the tissues indicated (pgWAT, perigonadal (visceral) WAT; iWAT, inguinal (subcutaneous) WAT; BAT, brown adipose tissue). Mice were housed either at thermoneutrality (TMN, 29 °C) or cool (10 °C); $n \geq 3$. **A** Radiolabel assimilation was calculated as dpm/mg tissue for the tissues indicated. **B** Calculated per organ (weights shown in Supplementary Fig. 2B), skins assimilated more label than any other tissue. Assimilation into iWAT was measured for the pair of iWAT depots, noting that there are 10 fat pads altogether in this class. With thermogenic fatty acid oxidation active (cool conditions), skin specific activity was reduced by 30%: **a**, comparison of skin from mice housed at TMN versus cool, $p = 0.0001$. **C** A scheme of the potential fates of 3H-triolein (acyl group 3H-label): acyl group reshuffling, fatty acid oxidation (FAO), degradation of acyl groups and dilution into general metabolic pool, or uptake of the whole TG moiety. These are not discriminated by assay of dpm/mg tissue. **D–J** Dilution and elimination of the radiolabel in BALB/cJ females is indicated for 2 weeks post-gavage (see also Supplementary Fig. 2, dpm/mg tissue, all data points; with statistics; $n \geq 3$). Timepoints shown are 2 h, 24 h, **3 days** (72 h), **1 week** (168 h) **and 2 weeks** (336 h) ($n \geq 3$ for each timepoint). **H** Comparison of impact of housing temperature upon label retention for 4 adipose-enriched tissues, 2 weeks after radiotracer administration (expansion of **D–J**). Data are presented as mean values +/− SD, significance is indicated by * (Methods) and exact p-values provided in the Source Data file.

females housed at either at thermoneutrality (29 °C; TMN) or at 10 °C (cool).

We found that the thermogenic depots iWAT and BAT[13] labeled to a 2-4x higher specific activity than other adipose depots, when mice were housed at thermoneutrality (Fig. 2A, Supplementary Fig. 2), and that skin labeled to approximately the same specific activity as visceral WAT (pgWAT). However, when the total incorporation of 3H-triolein label was calculated per organ (Fig. 2B, Supplementary Fig. 2B), we found that skin was the largest target for lipid delivery, irrespective of environmental housing temperature. Dedicated lipid storage depots (pgWAT and iWAT) showed only 20% (each) of the total acquisition and storage capacity of skin.

Comparable to other adipose depots, thermogenesis-associated lipid oxidation depletes skin TGs

Predictably, a single gavage of radiotracer was > 90% eliminated 1 week later from serum and liver (Fig. 2D, E; Supplementary Fig. 2). Elimination of the radiotracer was much slower for adipose depots than for serum and liver, and highly affected by housing temperature. Almost half of the maximum radiotracer was still present after 1 week (for both iWAT and pgWAT), substantially depleting only after 2 weeks for cool-housed mice (Fig. 2F–H; Supplementary Fig. 2). Surprised by the longevity of the label, we considered whether the gavage lipid dose could be higher than usual and therefore accumulating artifactually in skins. However, the dose administered was equivalent to only 50% of the lipid intake present in a daily ration of chow. Of all the adipose depots, BAT showed the highest rate of thermogenic oxidation (Fig. 2I), observed as the difference in radiotracer dpm for mice housed cool compared to warm.

Like these other adipose depots, skin showed rapid and progressive assimilation of dietary 3H-triolein during the first 24 h post-gavage (Fig. 2J; Supplementary Fig. 2). Radiotracer was depleted 2 weeks after cool exposure (Fig. 2J), suggesting that the triglyceride stores of skin can also be used to supply thermogenesis. The specific activity of female skin was 2-3-fold higher than for males, probably due to their higher relative dWAT content (40% compared to 16% total skin thickness; Supplementary Figs. 1, 2C).

Caloric restriction (CR) decreases dWAT and epidermis and reduces storage of dietary lipid in skin

The results shown in Fig. 2 suggest there is a mechanism for delivery of dietary lipids to skin. To determine whether this mechanism is regulated by a "healthy" dietary paradigm, we restricted food intake of mice, which is a well-established strategy that enhances metabolic health and longevity[14,15]: As expected, 30% CR for three weeks decreased body weight and reduced weight of adipose depots, including pgWAT and iWAT (Fig. 3A–C). CR also caused a dramatic reduction of dWAT in skin of male and female mice (Fig. 3D, E). Consistent with these observations, CR also lowered total TAG found in skin (Fig. 3F). Fate of dietary lipid was assessed 40 h after gavage of 3H-triolein, and amount of radiotracer stored in skin-associated lipids and TAGs was diminished in CR mice of both sexes (Fig. 3G, H). CR and decreased skin TAG was associated with a thinner epidermis, and a

lower mitotic index of the interfollicular basal keratinocytes (Fig. 3I, J). Together, these data illustrate that lipid delivery to skin is controlled, with profound impact on form and function.

Dietary TGs are delivered to both epidermis and dWAT

To determine which layer in the skin acquires dietary lipids, we separated skin into 3 fractions (Fig. 4A). These reflect the three distinct lipid-based thermal barriers in skin: the pelt/hair, coated in a sebome of mostly wax di-esters; the stratum corneum, a proteo-lipid cross-linked sheath of enucleated keratinocytes providing the top layer of the epidermis; and the dermal white adipose tissue (dWAT) underlying the pelt/epidermis/dermal layers (see Fig. 1I). Using enzymatic dissociation, we separated the dWAT from the dermal/epidermal layer (epi) of shaved skins to generate a highly enriched dWAT adipose fraction (Supplementary Fig. 10). These fractions (epi and dWAT) were labeled to approximately the same specific activity; 60% recovery from epidermal fraction, and 40% from dermal adipose (Fig. 4B). We conclude that 3H oleate can be acquired by the keratinocyte/sebocyte-enriched tissue fraction to a similar extent as the adipose depot.

To determine which lipid class had acquired 3H oleate, we isolated the lipids in sebome, skin, and separated skins (SS) by thin layer chromatography (TLC) and found that the triglyceride fraction of skin accounted for all detectable counts (Fig. 4C). There were no counts in the wax diester (WDE) or cholesterol ester (CE) fraction and label accumulation by hair was low/undetectable over the 2-week period. (Using this method, the TG fraction of BAT yielded the highest specific activity, as expected).

Tracing of dietary lipids using the MCFA content of milk fat

As an alternative approach to demonstrating that skin-associated lipids reflect dietary lipids directly, we fed mice with a Western diet (WD), enriched in the medium chain fatty acids (12:0,12:1,13:0, 13:1,14:0,14:1,15:0; MCFAs) typical of milk fat[16]. Analysis of diets using LC/QTOF-MS confirmed that MCFAs are absent from standard chow, in which soybean oil (60%) and grains are the fat sources (Supplementary Fig. 3).

Sera from mice fed WD for only 3 days showed typical changes, including increases in ceramides (CER), triglycerides (TG), phosphatidylcholines (PC), cholesterol esters (CE) and other phospholipids (Fig. 4D). Using LC/Q-TOF mass spectrometry, we identified TG species containing MCFAs in sera amongst the most most-changed group of lipids. MCFA-containing TGs appeared subsequently in epidermis (Fig. 4E, Supplementary Fig. 4A, B). The total amount of MCFA acyl chains significantly increased for all 3 fractions, dWAT, epidermis and sebome (Supplementary Fig. 4C).

An LPL-like enzyme is implicated in lipid uptake into skin

We tested whether dietary TG was delivered intact to skin, seeking direct matches between the circulating TGs that increased, and the increased species in epidermis ("skin"; Fig. 4F). We found many examples of MCFA-containing TGs that were increased in skin, but were not present, or did not increase, in the serum of WD-fed mice. This implicates a lipoprotein-lipase (**LPL**)-mediated acyl group
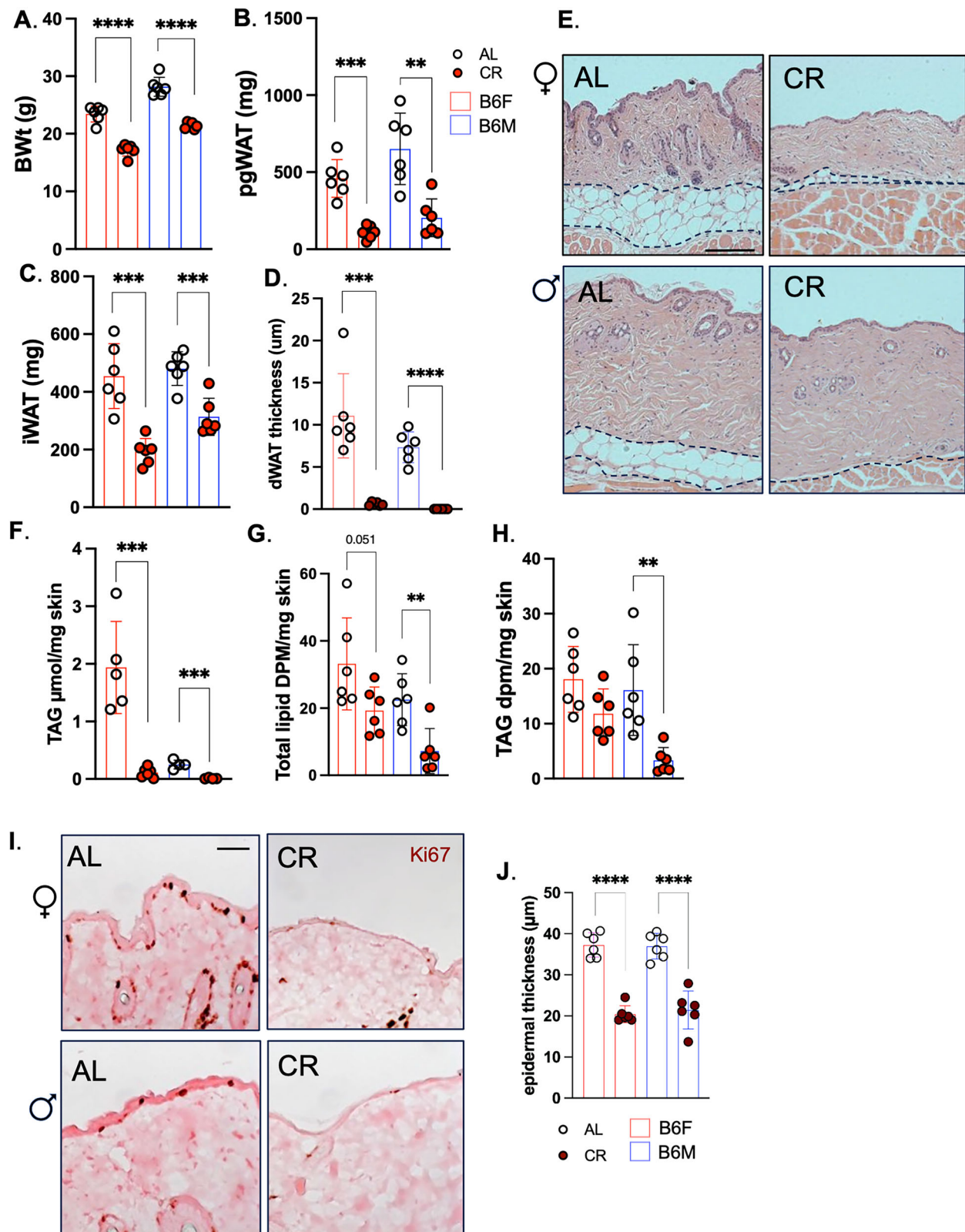
Fig. 3 | Caloric restriction decreases dWAT and epidermis and reduces storage of dietary lipid uptake in skin. Three weeks of CR diet reduced total body weight (**A**), pgWAT (**B**), iWAT (**C**) and dWAT thickness (**D**) of male and female C57BL/6 J mice (15–20 weeks old; $n = 6$). **E**. Representative H&E-stained sections from skins of mice fed AL or CR illustrate the thinning of dWAT quantified in (**D**). Scale bar=100 μm. **F**. Biochemical evaluation of TAG confirmed the reduction of TAG in skin from CR mice ($n = 5, 6$). The specific activity of total lipids (**G**) and TAGs (**H**) was reduced in skin of CR mice. **I** Mitotic indices of keratinocytes, evaluated by Ki67 staining of sections of paraffin-embedded skin samples, was reduced with CR, as was the thickness of the epidermis (**J**) of C57Bl/6 J male and female mice ($n = 6$). Scale bar = 25 μm. Data are presented as mean values +/− SD, significance is indicated by * (Methods) and exact p values are provided in the Source Data file.
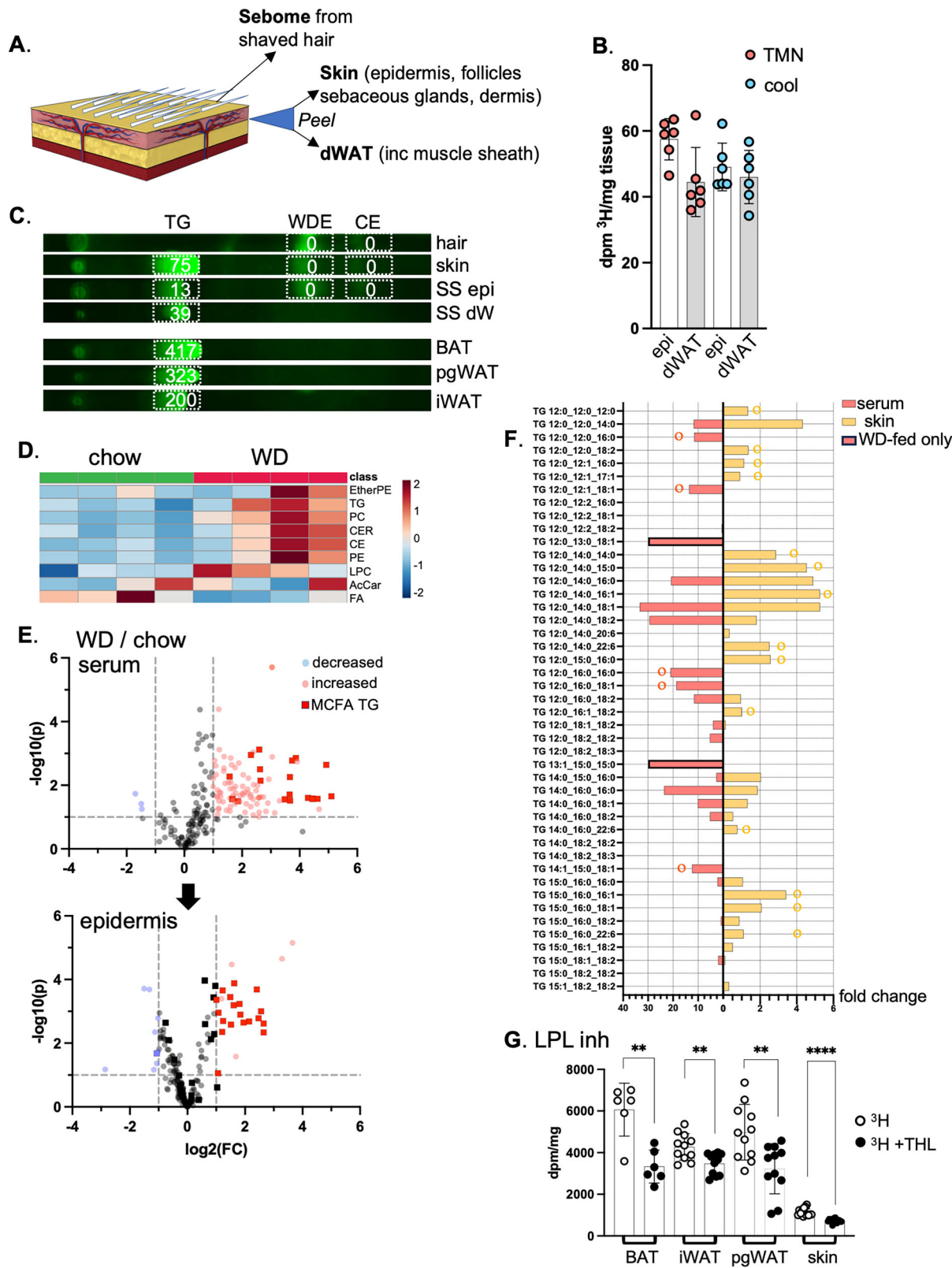
reshuffling in the delivery of TG-derived acyl chains to the skin epithelial cell population. We administered the lipoprotein lipase inhibitor, tetrahydrolipstatin (**THL**), one hour prior to 3H-triolein feeding and showed that uptake into skin was significantly reduced, alongside delivery to other adipose depots, pgWAT, iWAT and BAT (Fig. 4G). Therefore, LPL processing is likely to represent a rate determining step for the assimilation of TGs by skin.

Within 3 days of feeding low-isoleucine WD, skins become more heat permeable

Given that our data show increased insulative properties of skins after high fat-diet feeding, we asked whether skin insulative properties could also respond to health-promoting diet interventions. We and others have shown that, perhaps surprisingly, dietary protein restriction reduces fat mass and adiposity in both mice and humans[15–17].

Fig. 4 | Patterns of dietary delivery of acyl chains to skin. A−C *Radiotracer delivery to skin fractions*. Skin of BALB/cJ female mice (10-15 weeks old), labeled as for Fig.2 (^{3}H-triolein), was separated into 3 fractions, **sebome** (extracted from hair), **dWAT** (separated from skin), and the skin remainder (**epi; A**) and counted (**B**). The specific activity was approximately equal for epi and dWAT fractions for mice housed both at TMN or 10 °C (*n* = 3 mice; 2 readings/mouse). **C** Lipid classes were separated by thin layer chromatography (TLC), into triglyceride (TG), wax diester (WDE) and cholesterol ester (CE) and scraped for counting (an image of the TLC plate is shown annotated with dpm/mg tissue equivalent), from specific adipose depots from BALB/cJ females, along with hair, skin and separated skins (SS). All radiolabel was retrieved from the triglyceride fraction. **D−F** *Diet-derived MCFA delivery to skin*. **D** Feeding of Western diet for 3 days induces typical changes of circulating lipid classes, shown here for C57BL/6 J female mice (*n* = 4; WD or chow-fed). Data is shown as an unsupervised heatmap of sera samples (EtherPE ether phosphatidylethanolamines, PC phosphatidylcholines, Cer ceramides, CE cholesterol esters, PE phosphatidylethanolamines, LPC lysophosphatidylethanolamines, AcCar acyl carnitines, FA free fatty acids; *n* = 4). Scale for heat map is shown as fold change. **E** Volcano plots of the circulating lipidome and epidermis, showing significantly changed lipids (WD/chow), including TGs with medium chain fatty acids (MCFA), a signature of Western diet consumption (*n* = 4). **F** Fully specified MCFA-containing TGs were compared for serum and for skin, to test for a direct correlation of entire TG species (implicating direct delivery). Species indicated with o or o are unique to either serum or skin (respectively) or are present only in serum (WD-fed only). **G** Specific activity of adipose depots and skins from C57BL/6 J female mice administered tetrahydrolipstatin (THL, lipoprotein lipase inhibitor) before radiotracer administration (*n* = 3 mice; 2–4 readings/tissue/mouse). See also lipid profiles of diets (Supplementary Fig. 3) and MCFA distribution and relative content in serum, epidermis and sebome (Supplementary Fig. 4). Data are presented as mean values +/− SD, significance is indicated by * (Methods) and exact *p* values provided in the Source Data file.

Specifically, adiposity is promoted by branched-chain amino acids (BCAAs); restriction of all three BCAAs or isoleucine alone rapidly restores leanness to male mice with diet-induced obesity (DIO), associated with increased energy expenditure and better glycemic control[15,18].

To demonstrate the effect of isoleucine restriction in female mice, we switched the diet of C57BL/6 female mice made obese by 16 weeks of WD consumption, to a diet with low isoleucine (**WDIL**) or low branched chain amino acids (leucine, isoleucine and valine, all at 33% of standard amounts, **WD 1/3xBCAA**; Fig. 5A, B; Supplementary Fig. 5). The diets all contain identical amounts and sources of fat and sugar; calories removed through reductions of BCAAs are replaced with non-essential amino acids to maintain the diets as isocaloric (Table S1). We found that mice lost weight on WDIL diet, achieving a lean weight within 3 weeks (Fig. 5A). Analysis of body composition showed that the weight reduction in mice fed the BCAA and Ile-restricted diets primarily resulted from reduced fat mass (Fig. 5B, Supplementary Fig. 5).

To test whether loss of heat through skins could contribute to the rapid weight loss induced by this low-isoleucine diet, skin function was assessed for C57BL/6 female mice fed WD or WDIL for 3 days. Over this short timeline, mice fed WDIL adjusted their calorie intake to match chow-fed animals, where mice fed WD consumed 40% more calories (Fig. 5C, D). Mice eating WDIL did not show the suppression of water intake induced by WD consumption (Fig. 5E). After only 3 days of feeding, mice eating WDIL lost over 1 gram of body weight (Fig. 6F). Mice eating Western diet showed no significant body weight increase at this time point, however, pgWAT adipocytes were already larger, and BAT adipocytes contained a higher lipid load (Fig. 5G); mice eating a WDIL diet resisted these changes, and dWAT thickness was already trending down (Fig. 5H).

Skins and pelts from WDIL-fed mice showed increased rates of evaporative cooling; TEWL was increased by 25% and 40% respectively (Fig. 5I, J). The insulation measured by FLIR was reduced (Fig. 6K). We conclude that within days of diet switch, WDIL-fed mice are protected from the obesogenic effects of WD-feeding and this is associated with the rapid development of heat-permeable skins. Note that in contrast to mice fed HFD, skin from mice fed WD show no net change in skin properties after 3 days feeding.

Multimodal lipidomic analysis of dWAT, epidermis and sebome

We turned to lipidomics to identify molecular correlates of altered thermal barriers. Each of the biomaterials comprising the skin thermal barrier depends upon different processes of lipid biosynthesis for their properties (Fig. 6A). Specifically, TGs comprise most of the lipids of dermal WAT; the sebome is synthesized by sebocytes (ancillary to the hair follicle and derived from epidermis) and comprises mostly wax diesters[19]. The epidermal stratum corneum is made by keratinocytes and comprises a cross-linked proteolipid matrix with abundant ceramides. We applied a LC/QTOF-MS untargeted lipidomics pipeline in both positive and negative modes, to identify and quantify unique lipid species[20] (Fig. 6B). Although it is likely that neutral lipid species are important to thermal properties, the predominant wax diester (WDE) species of sebome are not identified by standard lipid annotation programs. Therefore, in order to report on this fraction, we separated WDE by TLC (see TLC profile of Fig. 4C), derivatized the acyl groups to fatty acyl methyl esters (FAMEs) and characterized the products using GC/MS. One notable exception to the lipids assayed using this multimodal approach is cholesterol, which is a major component of the stratum corneum[21,22].

Serum, skin and sebome present almost exclusive ceramide profiles (Supplementary Fig. 6); this likely reflects the different functions of ceramides, as signaling molecules, precursors to the cross-linked ceramide sheath comprising mammalian skin, and components of the thermal barrier coating mouse hair, respectively[2,19,20,23,24]. Skin has the most ceramide/mg tissue, though hair/sebome shows similar abundance. Overall, most ceramide species in sebome and skin are hydroxylated (α- or β-) sphingosines and dihydro-sphingosines[21,22] (Supplementary Fig. 6). Ceramides are crucial to epidermal barrier function, and specific ceramide species have different potency in the performance of the stratum corneum[19,25].

Three days of feeding HFD increases several lipid types in sebome and epidermis

Using separated skins from mice fed HFD for 3 days, we analyzed the lipid fraction of BALB/cJ male and female hair-associated sebome and epidermis (Fig. 6B, C). Both epidermis and sebome were significantly changed by high fat consumption, characterized as a widespread depletion of approximately 20% of all lipids in the epidermis, and a corresponding gain of lipids secreted onto the pelt. Although the simplest explanation for this symmetry would be that the sebocytes empty their contents onto the pelt, we compared the lipids appearing in sebome with the lipids depleted in epidermis and found they were not the same. This suggests that epidermal lipid depletion is associated with a more generalized alteration and activation of keratinocyte function[26].

The TGs present in the hair fraction increased by 70% (both male and female) and were distinguished from the changes in other lipid classes by their larger accumulation (Fig. 6B). This was observed by both lipidomics and TLC. Furthermore, TAGs became enriched in saturated acyl chains and depleted in poly-unsaturated acyl chains (Fig. 6D). Thus, males fed HFD show an increase of 5.5% saturated fatty acids (from 27% total in control fed condition; SFAs), and a decrease of 8.4% (from 48.5% total; PUFAs), where females show a similar, muted trend. Given that increased acyl chain saturation changes the melt temperature and physical properties of TGs, this may contribute to significant functional change.

For the epidermis, the only lipid class that did not become depleted were the ceramides. Mass spectrometric assay can measure
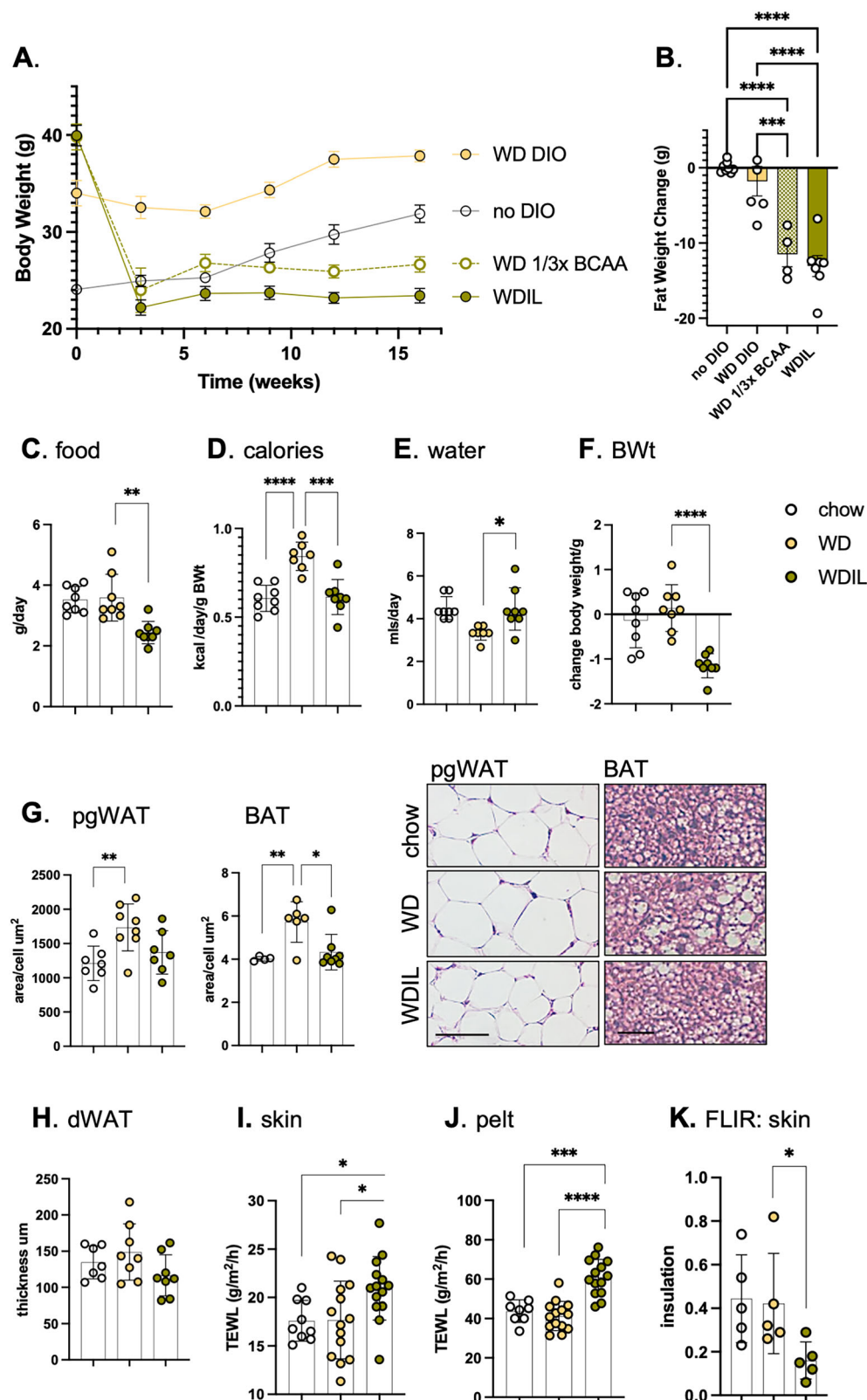
only the soluble ceramide pool, the precursors to the assembly of the highly insoluble and cross-linked stratum corneum[27]. Thus we cannot quantify the amount of stratum corneum present, but can only speculate that given the precursor pool was increased, the amount of stratum corneum was likewise increased. Ceramides present in the sebome increased by approximately 20% across all 8 classes identified (Fig. 6E). The changes of ceramide amount were higher for males than

females, a pattern that correlated with the exacerbated pelt insulation for males fed HFD (Fig. 1E). Baseline amounts of ceramides in females were >2-fold higher.

Surprisingly, even the wax diesters coating the pelt were affected by short exposure to HFD diet consumption. Hair goes through a month-long asynchronous process of growth and involution[28], implying that hair lipids could be stable and unchanging. However, we found

Fig. 5 | Mice fed a low-isoleucine Western diet rapidly develop heat-permeable skins. A, **B** *Impact of WDIL diet feeding.* C57BL/6 female mice made obese by 16 weeks of WD feeding (**WD DIO;** TD.88137), were switched to low isoleucine (**WDIL**; TD.200692), low branched chain amino acid (**WD 1/3xBCAA**; TD.200691), or amino acid-defined WD (**WD DIO**; TD.200690). A control cohort were maintained on a regular fat content diet for the duration (**no DIO;** TD200693). Body composition was measured 3 weeks post diet-switch (see also Supplementary Fig. 5 for lean/fat body composition), showing loss of 15 g body fat within 21 days. Each data point represents a mouse (*n* = 4–6). Data in (**B**) was analyzed using a one-way ANOVA test. **B**, **C** *Rapid response to WDIL feeding.* To test the impact of a switch to WDIL consumption, female C57BL/6 J mice (10–15 weeks old) were switched to Western diet (**WD**) or low-isoleucine Western diet (**WDIL**) for 3 days, and daily water and food consumption assessed (expressed as both grams/day or kcal/day/g body weight; **C–E**, *n* = 7, 8). **F** Body weights were measured after 3 days. **G**, **H** Changes to adipocyte depot lipid loads were calculated as the average area of pgWAT adipocytes, thickness of dWAT, or the lipid droplet area/cell for BAT, shown also as representative H&E-stained skin sections (*n* = 6–8). Scale bar=50 µm. **I–K** TEWL and FLIR assays of thermal barrier function for mice fed chow, WD, or WDIL for 3 days (TEWL measured from 2 skin samples each from 5 to 7 mice; FLIR assay; *n* = 5). Data are presented as mean values +/− SD, significance is indicated by * (Methods) and exact *p* values provided in the Source Data file.

that WDEs accumulate over 3-fold on the coats of mice fed HFD (Supplementary Fig. 8C), suggesting that the wax coating is labile. FAME analysis of the acyl-groups present in sebome WDE lipids shows a diverse group of at least 35 species, some tentatively identified using co-migration with standard species (Supplementary Fig. 7). This group is likely to include hydroxylated, very long and desaturated isomers of the more common standards. There is little change of composition induced by high fat feeding, instead there is an increase in total amount of WDEs. There are 10 long chain acyl groups that comprise 90% of total (Supplementary Fig. 7). The complexity of the assembled WDE class could therefore be vast, given that each lipid includes at least 3 acyl groups. Thus, we propose that the reduction of complexity by FAME derivatization is the method of choice, giving better insight than their partial identification and quantitation in LC/QTOF-MS spectra.

The changes we observed in skins of mice fed HFD for 3 days are summarized in the scheme of Fig. 6F: increased wax diesters on hair, increased ceramides in skin, increased sebocyte activity, with excretion of excess triglycerides and remodeling of the secreted triglycerides to be more saturated.

Three days of feeding low-isoleucine WD suppressed changes associated with WD and suppressed key signaling lipids

By way of contrast, we analyzed the hyper heat-permeable skins from mice fed WDIL using the same techniques (Supplementary Fig. 8, total inventory of lipids identified). We found that WDIL-fed mice partly resisted the increase in MCFA-containing circulating lipids that accompanies WD consumption, and completely resisted delivery and accumulation of MCFAs in skin (Fig. 7A, B). Other changes in circulating lipids were reduced or prevented in WDIL-fed mice, including the phosphatidylcholines (and associated lysophosphatidylcholines), ceramides, sphingomyelins, and cholesterol esters (Fig. 7B), leading us to conclude that low isoleucine-containing diet consumption leads to a profound alteration of the processing of WD by gut and/or liver.

For WD-fed mice, 25% of the epidermis-associated reservoir of inflammatory oxylipid precursor acyl chains stored in TGs was mobilized, notably arachidonic acid (20:4) and linolenic acid (20:3; Fig. 7C); this change was prevented in mice fed WDIL. There were also distinctive lipid changes in the epidermis of WDIL-fed mice, such as a depletion of acyl carnitines, phosphatidylethanolamines and related species of ether-linked phosphatidylethanolamines (Ether PEs), and ether-linked oxidized phosphatidylcholines (EtherOxPCs) (Fig. 7D–G). Acyl carnitines are key transporters of long chain fatty acyl chains during fatty acid oxidation[29]; PEs, Ether PEs and EtherOxPCs are peroxisomal in origin and are known to be important to lipid raft function[30].

Similar to HFD-feeding, skins from WD-fed mice showed a broadly similar trend towards sebome lipid elevation with corresponding depletion of total lipids from epidermis. Interestingly, given that WDIL feeding appears to prevent most other changes, WDIL-fed mice also show increased lipids in the sebome. Unlike HFD consumption, the relative secretion of TGs was not increased above all the other lipid classes, therefore excess fat does not tend to vent out through the skins of WD-fed mice (Fig. 8A, B).

Surprisingly, and in contrast to the response to HFD-feeding, WD-feeding reduced the amount of hair-associated wax diesters by nearly 80%, and mice fed WDIL-diet resisted this phenotype (Fig. 8C).

In summary (Fig. 8D), skins from WDIL-fed mice resisted some of the changes induced by WD-feeding, including delivery of dietary lipids, mobilization of oxylipid reserves and remodeling of wax diesters. However, this diet also induces novel responses, including reduced amounts of specific signaling lipids: together these molecular changes are associated with increased skin heat permeability. These studies reveal that skin reflects diet rapidly and profoundly, with potential for changing energy expenditure overall.

Discussion

Skin is a major target for dietary lipids, and uptake is regulated

We have shown that skin is the dominant destination for triglyceride acyl chains, indeed more so than other individual tissues, including adipose and liver. Skin can store dietary fats for weeks after consumption; along with iWAT and BAT depots, skin shows a higher rate of mobilization and oxidation in thermogenically active mice (i.e. mice in sub-thermoneutral housing).

Triglyceride radiotracer was assimilated both by dWAT and by the epidermis, where the latter is known to rely upon TG stores for the massive biosynthesis reactions required to make the stratum corneum[26]. Furthermore, we show that caloric restricted mice show almost no uptake of ³H triolein by skin, and we conclude that triglyceride uptake into skin is a regulated process. Lack of triglyceride uptake has profound consequences for the skins of caloric restricted mice, leading to a dramatic epidermal thinning, and depletion of adipocytes in dWAT. A published study from Kowaltowski[31] showed that after 6 months of caloric-restriction, mouse pelt became more dense and packed with guard hairs; this hair regrowth was supported by an increase in the activity of follicular stem cells. The surface temperature of the skin was lower, and indeed, the cold stress induced by shaving these highly pelt-dependent mice forced them into muscle protein oxidation and metabolic distress. This implies that skin/pelt is a highly homeostatic organ, with means to compensate for excessive heat loss.

Given that skins become so highly lipid depleted by calorie restriction, it may not be surprising that calorie restricted rats show poor skin wound healing[32]. Subcutaneous and dermal WAT depots have been shown to be mobilized during wound repair in mice, and this mobilization is required to promote extracellular matrix production by dermal fibroblasts and healing[29,30,33,34]. Hair growth is regulated by intermittent fasting and by gastric sleeve surgery[35,36]. We speculate that poor lipid uptake into skins may underlie the deficiencies observed during wound healing of diabetic patients[37], and propose that, like adipose, skin could have an important role in the uptake of other circulating metabolites, including other lipids, glucose and branched chain amino acids[38].

Our data suggests that LPL is involved in uptake of dietary acyl groups into skin, along with other better-studied adipose depots[39], but we anticipate there will be other processes of metabolite delivery to maintain the high level of de novo lipogenesis characteristic of sebocytes and keratinocytes. Wellen and colleagues showed that intrinsic
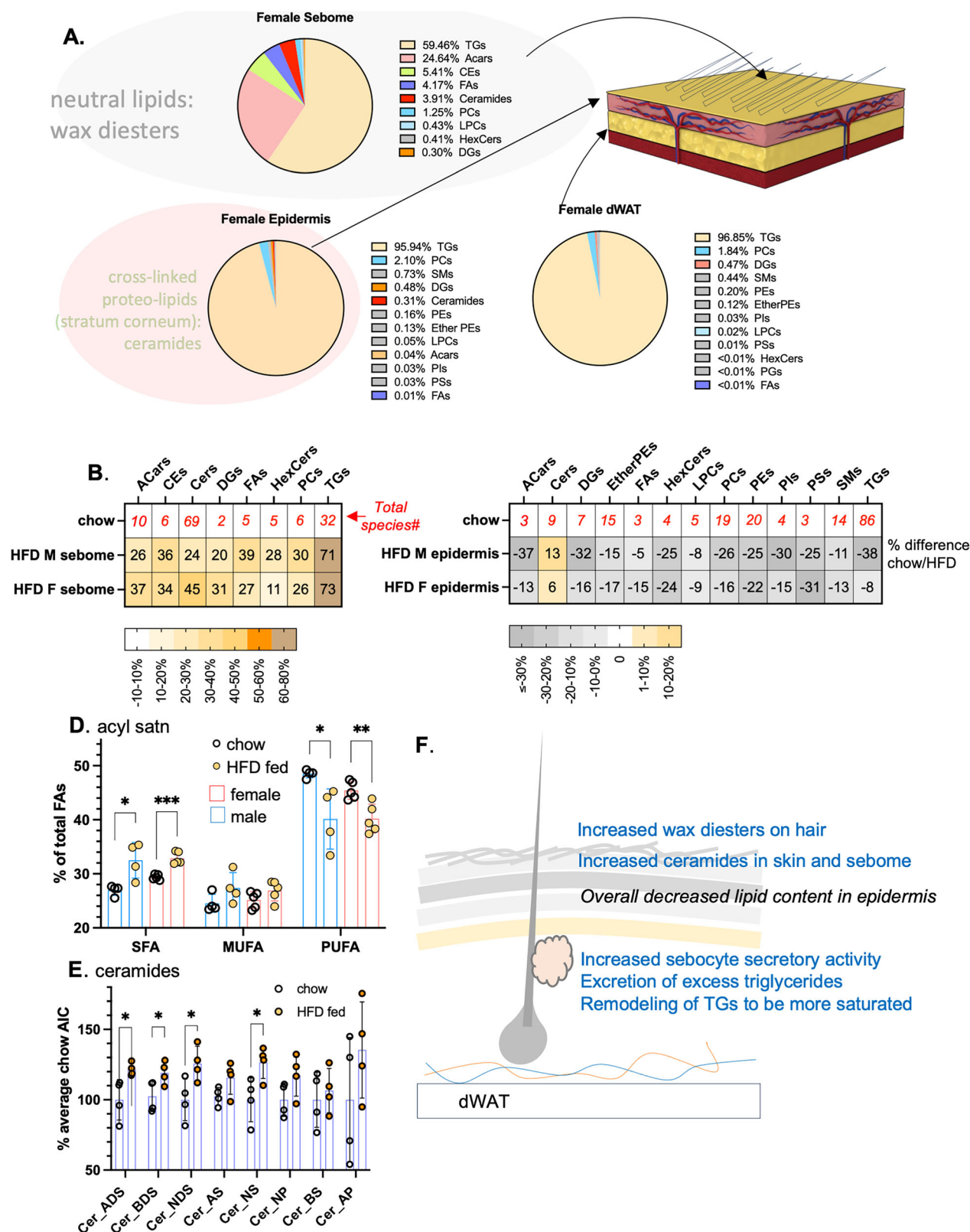
defects of de novo lipogenesis can be rescued by the addition of dietary lipids, and furthermore, that decreased stratum corneum barrier function induces compensatory reactions in sebocytes[40]. The effect of diet on skin functions may be mediated not only by direct uptake of dietary lipids, but by the signaling activity of the gut-skin axis[41–43].

It will be important to assess dietary lipid uptake into human skin. We have shown that there is little or no dWAT equivalent in human subjects, defined as a β-adrenergic-resistant depot associated with skin[44]. The regulation of skin-associated fat (SAF) in human may more closely resemble mouse scWAT. For lean women, SAF is estimated to be the largest adipose depot, varying between 6.5 -15 mm thick for individuals (an average of 15.8 kg) in a manner little related to general adiposity. Its regulation could be key to understanding personal energetics. Other studies of human adipose, specifically human

Fig. 6 | High fat diet consumption results in changes to components known to be thermally active in both sebome and skin lipidomes. A *Multi-modal lipid analysis of skins* (see also Supplementary Figs. 6, 7). Skin tissue fractions (produced as described in Fig. 4 and Materials and Methods) were analyzed for their lipid composition using LC/Q-TOF mass spectrometry. The larger grey circle shown around the sebome indicates the neutral lipid wax esters (and potentially other classes) which are under-annotated by mass spectrometry (compare with TLC separation of Supplementary Fig. 6B). The larger pink circle around the epidermal lipids indicates the cross-linked proteolipid sheath called the stratum corneum, highly enriched with ceramides, which is not solubilized by these methods, therefore not detectable. **B, C** The relative abundance (HFD/chow) of each lipid class is shown for sebome and epidermis from both BALB/cJ males and females (using AUC for this comparison). The HFD/chow ratio is calculated for males and females separately, since their skins are so different. The numbers in red along the top row show the total number of species compared for each class (*n* = 4; additional lipid abbreviations noted here are DGs, diacylglycerols; HexCers, hexaceramides; PIs, phosphoinositides; PSs, phosphoserines; SMs, sphingomyelins). **D** Acyl chain saturation (summed from all lipid species), showing saturated fatty acids (**SFA**), mono-unsaturated FAs (**MUFA**) and poly-unsaturated FAs (**PUFA**) as % of total, for sebome of chow or HFD-fed males and female BALB/cJ mice (n = 4). **E** The most abundant 5 ceramide classes in sebome of HFD-fed male BALB/cJ mice increases by approximately the same degree (*n* = 4). See also Supplementary Fig. 6 for description of ceramide species detected in serum, epidermis and sebome (almost mutually exclusive). **F** Summary scheme of the changes of sebome and epidermis observed in response to HFD feeding. Data are presented as mean values +/− SD, significance is indicated by * (Methods) and exact *p* values provided in the Source Data file.

---

visceral adipose tissue, showed slow TG turnover[45,46], where turnover was regulated by β-adrenergic, insulin and other endocrine factors.

How important is thermal adaptation of skin to insulation, energetics and metabolic health of mammals?

Our data shows that diet can induce rapid changes in the functional insulating properties of skin. Within only 3 days, high fat diet increases insulation (measured experimentally), and reduces heat lost by evaporative cooling by up to 28%, as measured for skins with or without hair, from both sexes of BALB/cJ and C57BL/6 J mice. Since the consumption of high fat diet promotes skin-associated insulation, this could exacerbate the obesogenic effects of high fat consumption, by reducing the overall need for thermogenesis.

A prior publication made a sweeping conclusion that there was no change of insulation caused by obesity[46,47] (with a counterpoint publication describing obese humans published by Brychta et al.[48,49]). In that study, obese and normal weight mice were compared for their relative consumption of O_2 when housed at different environmental temperatures, and a number of assumptions applied to calculate "insulation". The shortcomings of conclusions based on the Scholander equation were described in detail by Dr. John Speakman[50]. We conclude that skin thermal properties should be measured directly, using modern techniques, to test the physiological basis of skin-derived cues[51].

Which lipid components correlate with altered thermal barrier function?

Three days post diet-switch, there were already molecular changes in both the sebome and epidermis but none in dWAT: we suggest that dWAT acts as a more chronic adaptive response[47]. The observed gain of stratum corneum-associated ceramides[25] and a trend to a more saturated acyl chain content are predicted to lower heat transfer. More novel perhaps are the changes we observed in the neutral wax diester classes which coat the skin and hair. Although hair only renews approximately monthly in an asynchronous pattern of replacement[5,48], the wax diester coating was increased by > 3-fold upon HFD-feeding. In contrast to this gain of insulation, feeding of a low isoleucine diet led to skins with increased heat permeability, associated with specific losses of lipids with signaling functions in the epidermal fraction. Taken together, these data suggest that thermal barrier function has contributions from several cell types.

Which cellular components are implicated in functional responses?

Our study describes an acute modification of skin function: this is led by changes in the lipid products made by both keratinocytes and their differentiated derivatives, sebocytes. It is likely that both cell types are responsive and collaborative. Sebocytes have been called the brain of the skin[49], due to their ability to integrate and process different cues, and they comprise some 2% of body mass. They are highly connected to neural and endocrine networks, have a high energy requirement,

and their lipid products are important not only for hair shaft eruption but provide a signaling role to the skin cell community, providing feedback regulation of their own activity[50].

Does skin offer a means of excess lipid disposal?

Skin is highly regenerative and the ceramide component of stratum corneum is continuously shed (with a half-life of 7–10 days). Ceramides are biosynthesized from triglyceride stores assembled by keratinocytes[19,26], and together these could provide a significant route for elimination of excess lipid. Sebome secretion too provides a vent for excess dietary triglycerides, here increasing by 70% in mice fed high fat diet. We estimate that the whole pelt of a chow-fed mouse contains approximately 10 mg of TG, compared to 17 mg for a mouse fed HFD (assuming a total 200 mg hair per pelt). A pattern of triglyceride venting through sebome was suggested by Choa et al. to be a major route for excess triglyceride secretion induced by the cytokine thymic stromal lymphopoietin (tslp)[51]. Although unlikely to account for the approximately 15 g of adipose-associated triglycerides lost during the 3 weeks of this study, sebome-associated triglyceride levels could be an important biomarker for circulating triglyceride levels and/or changing energetics. Over-production of skin TGs was also noted after exposure to *acnes* bacteria[52].

Western and high fat diet promote different changes in skin

Skins from mice fed WD showed no net change in skin properties after 3 days feeding diet; this is associated with lack of accumulation of epidermal ceramide precursors and a dramatic reduction in sebome-associated WDE. These diets have different fat contents (calories from fat are 60% for HFD, 42% for WD and 18% for chow), however, WD combines high sucrose (34% w/w) with elevated fat content, a combination shown to be highly pro-inflammatory, both in general and for skin specifically[53–57]. For example, WD feeding exacerbated susceptibility to the TLR7 agonist imiquimod, leading to the development of psoriasiform dermatitis. A study of the molecular basis of balding induced by fish oil consumption revealed a clear direct relationship between dietary lipids, skin immune cells and their specific recruitment to the hair follicle[58].

We found large reservoirs of oxylipid acyl precursor chains immobilized in the triglyceride fraction of epidermis, of which 25% are released during the first (3-day) exposure to WD consumption. These include 22:6, 20:4, and 20:3 acyl chains, all precursors to the inflammatory lipokines (prostaglandins, leukotrienes and thromboxanes). It is tempting to draw a conclusion that this mobilization provides the substrates for the triggered inflammatory reaction characteristic of skins from WD-fed mice.

Skin changes in low-isoleucine fed mice reflect major changes in diet disposition

The functional changes of skins from mice fed WDIL diet coincided with a loss of about 1 g of body weight over the course of 3 days, which
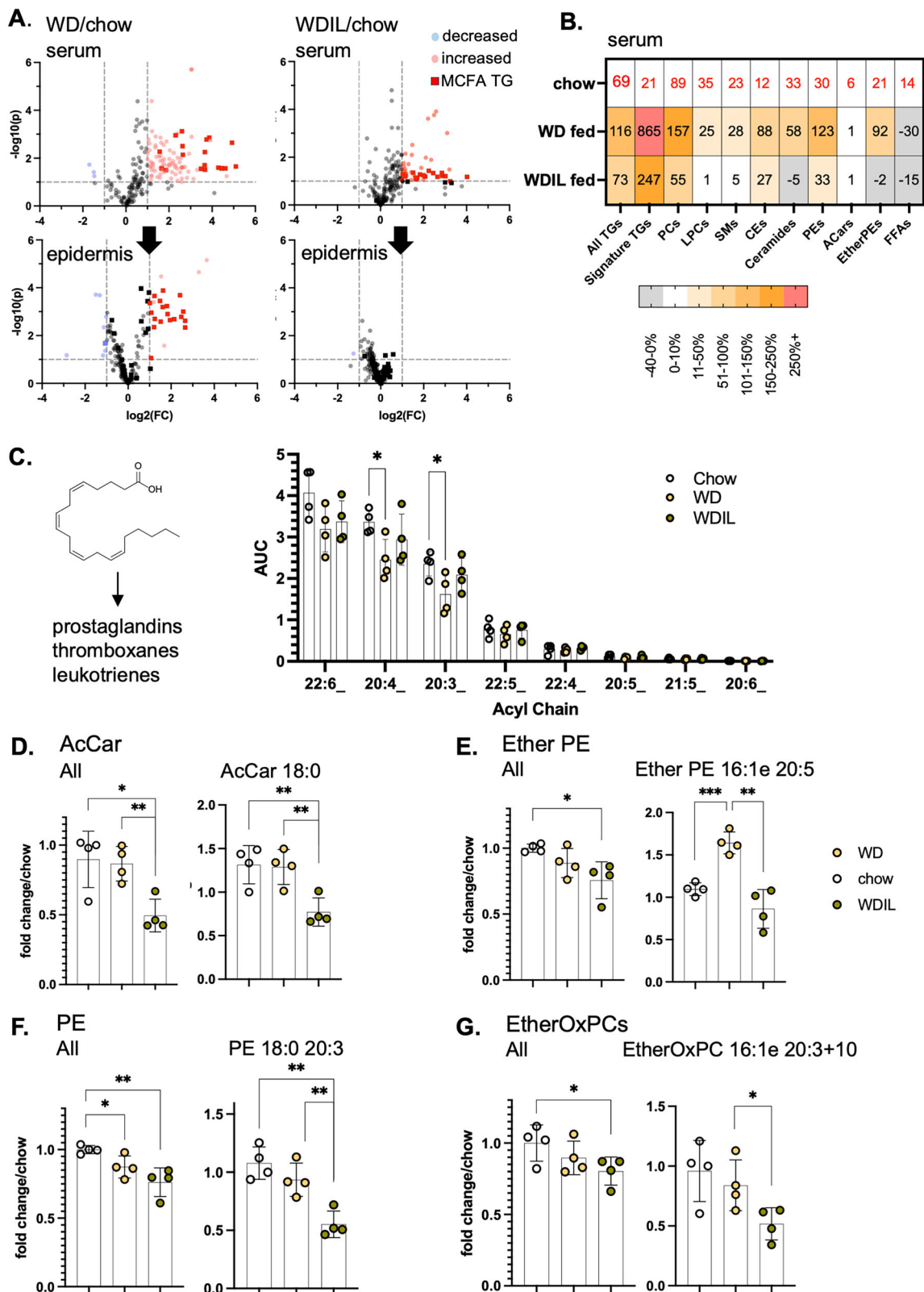
Fig. 7 | Low isoleucine Western diet prevents dietary delivery of acyl chains, mobilization of pro-inflammatory oxylipids from the epidermal reservoir, and suppresses specific signaling lipids. A Relative appearance of Western-diet enriched MCFAs in epidermis of WDIL-fed C57BL/6 J female (10–15 weeks old) compared to WD-fed mice (see also Fig. 4; $n = 4$). **B** Heatmap of changes induced in circulating lipids for WD- and WDIL-fed animals. **C** Oxylipid acyl chains, precursors of inflammatory cytokines (shown left hand side) were quantified for epidermal fractions from mice in all 3 diet conditions. **D–G** Low isoleucine-fed mice show lower levels of several classes of lipids associated with signaling functions ($n = 4$; shown here for C57BL/6 J female mice). Illustrated are the trends present for the entire class, followed by a specific example of each. Data are presented as mean values +/− SD, significance is indicated by * (Methods) and exact p values provided in the Source Data file.
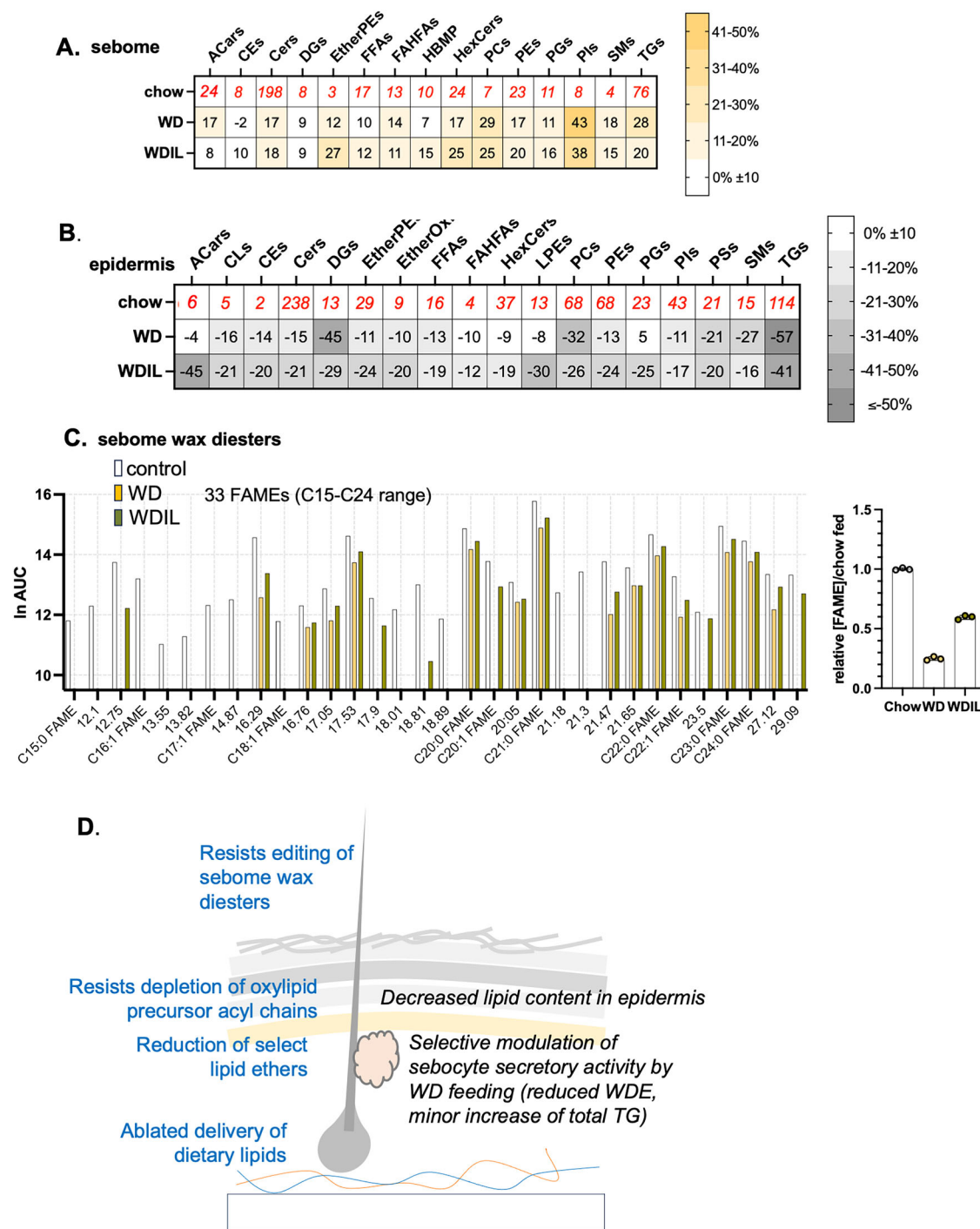
A. sebome

	ACars	CEs	Cers	DGs	EtherPEs	FFAs	FAHFAs	HBMP	HexCers	PCs	PEs	PGs	PIs	SMs	TGs
chow	24	8	198	8	3	17	13	10	24	7	23	11	8	4	76
WD	17	-2	17	9	12	10	14	7	17	29	17	11	43	18	28
WDIL	8	10	18	9	27	12	11	15	25	25	20	16	38	15	20

B. epidermis

	ACars	CLs	CEs	Cers	DGs	EtherPEs	EtherOx.	FFAs	FAHFAs	HexCers	LPEs	PCs	PEs	PGs	PIs	PSs	SMs	TGs
chow	6	5	2	238	13	29	9	16	4	37	13	68	68	23	43	21	15	114
WD	-4	-16	-14	-15	-45	-11	-10	-13	-10	-9	-8	-32	-13	5	-11	-21	-27	-57
WDIL	-45	-21	-20	-21	-29	-24	-20	-19	-12	-19	-30	-26	-24	-25	-17	-20	-16	-41

C. sebome wax diesters

D.

Fig. 8 | Summary of changes of heat-permeable skins induced by feeding low isoleucine diet. A, B Relative abundance of each lipid class is shown for C57BL/6 J male sebome and epidermis, for control, WD and WDIL-fed mice (*n* = 4). See also Supplementary Fig. 9, inventory of total species interrogated. **C** Wax diester ester (WDE)-derived FAME mixtures were extracted from 3 independent mice and pooled for analysis by GC-MS. Mice fed WDIL diet resisted the depletion of WDEs observed after WD-feeding (see also Supplementary Fig. 7, waterfall plot). Data are presented as mean values +/− SD, significance is indicated by * (Methods) and exact *p* values provided in the Source Data file. **D** Summary scheme of the changes of sebome and epidermis observed in response to WD/WDIL feeding.

we have previously shown to be the new, lean, steady state for these mice[15,18]. Sera from WDIL-fed mice revealed that low isoleucine can prevent the changes of circulating lipids that are typical of WD-consumption (elevation of phosphatidylcholines, sphingomyelins and ceramides). Likewise, uptake of dietary acyl chains to skin is prevented by low isoleucine feeding. However, low isoleucine diet does not merely prevent distribution of dietary lipids, the skins show a specific signature loss of lipids with signaling roles, including acyl carnitines,

phosphatidylethanolamines and ether lipids such as ether phosphatidylethanolamines[59–61], suggesting the induction of a specific signal.

Overall, we conclude that dietary lipids are taken up and stored by skins where they alter the properties of those skins, with potential to modulate animal insulation and energetics. We have shown that a "health promoting" diet is associated with increased heat loss through skins, whereas an obesogenic diet is insulating. Testing of other dietary

paradigms will show how widespread this phenomenon is. Diet could modify the thermal properties of skins either directly, by incorporation into thermally-active lipids, or indirectly, via signaling to cells of the skin, including neurons. The molecular changes documented here implicate diet as a modulator of both sebocyte and epidermal keratinocyte functions, where each is responsible for a different component of the thermal barrier.

Methods

Ethical Approval

These studies were performed in strict accordance with the recommendations in the Guide for the Care and Use of Laboratory Animals of the National Institutes of Health. Experimental protocols were approved by the University of Wisconsin School of Medicine and Public Health Institutional Animal Care and Use Committee (IACUC) and the William S. Middleton Memorial Veterans Hospital IACUC. The number of mice used to perform this study was minimized, and every effort was made to reduce the chance of pain or suffering. All authors understand the ethical principles and confirm that this work complies with the animal ethics checklist.

Mice

Mouse strains and sexes are specified in the results and figure legends: C57BL/6 J (Jackson labs cat#00664) and BALB/cJ (Jackson labs cat#00651). For routine housing, mice were housed at constant temperature (19–23 °C) in 12 h light/dark cycles with free access to water. The diets used were standard chow (Harlan Teklad Global Diet 2018), high fat diet (HFD; Envigo diet# TD.06414, 60% calories from fat); amino acid-defined Western diet (41% calories from fat, 21% w/w milk fat, 34% sucrose, Envigo diet# TD.160186) and a matching diet with low isoleucine (67% reduced (0.254%) isoleucine, Envigo diet# TD.170484), as described by Lamming and colleagues[15,18]. To demonstrate the long-term impact of low isoleucine diet consumption on mice with diet-induced obesity (DIO), C57BL/6 J female mice were pre-conditioned by feeding a Western diet for 16 weeks (TD.88137), where the non-DIO cohort remained on a control diet (no DIO; TD.200693). Then WD-fed mice were divided between amino acid defined (AAD) Western diets containing low branched chain amino acids (WD 1/3x BCAA WD; TD.200691), only low isoleucine (WDIL; TD.200692), or standard amino acids (WD DIO; TD.200690). Full diet descriptions, compositions and item numbers are provided in Supplemental Table 1.

Assay of skin thermal properties: transepidermal water loss (TEWL) and forward-looking infrared surface thermography (FLIR)

Half of the dorsal skin was shaved, and a strip of skin (approximately 3 × 2 cm) excised and assayed promptly for functional properties. Areas of skin obviously in anagen (appear black on underside for C57BL/6 J skins) are not used for assay. Samples were transferred to a heat block protected from air flow, and held at 34 °C; at least 7 TEWL readings were taken using a Vapometer probe (Delfin) of skin placed on a wet Wypall on the heat block, as previously described[6]. FLIR was measured using a FLIR One Pro camera plug-in for an iPhone, which is internally automatically calibrated. At least 10 pictures were taken to read out skin surface temperature together with near adjacent heat block temperature, and the difference read out as (arbitrary) °C insulation.

Caloric restriction, non-standard housing and metabolic phenotyping

For caloric restriction experiments, C57Bl/6 J mice (both males and females; 16 weeks of age) were singly housed and fed ad libitum (**AL**) with control diet (D17110202; Research Diets) or caloric-restricted (30% **CR**, D19051601; Research Diets)[62] for 3 weeks at room temperature (22 °C). The method used for evaluating radiotracer uptake had minor modifications (Supplementary Fig. 9). For experiments with non-standard housing temperatures, mice were singly housed in environmental chambers (Memmert HPP750 or Caron 7350). Temperatures used were either thermoneutrality (**TMN;** 29 °C, 30% RH) or **cool** (10 °C, 30% RH), as described previously[63]. Many studies use thermoneutral temperatures > 30 °C; we use 29 °C to eliminate significant changes to breeding or exercise behavior. We have not demonstrated that this temperature is thermoneutral for mice with acutely altered skin properties, however, the rate of thermogenesis (measured by BAT activation) is much reduced compared to the cool condition. For longer term experiments, mice were weighed weekly and body composition determined using an EchoMRI Body Composition Analyzer.

Histological analysis

Skin, BAT, perigonadal WAT (pgWAT) and the inguinal (mammary) subcutaneous fat pads (iWAT) were dissected for histological processing as described in Kasza et al.[44]. Briefly, paraformaldehyde-fixed, paraffin-embedded samples were H&E stained and assayed as follows: 1) dWAT thickness: 6 images of H&E-stained, non-anagen fields of skins (equivalent to ≥ 4500 μm linear dWAT) were assayed by image analysis (dividing total area by length). 2) Assay of BAT lipid stores: Lipid droplets were identified in gray scale images using circularity (0.1–1.0) and diameter (0.1–50 μm) thresholds in 6 independent fields of BAT (> 1200 cells) and quantified using the open-source Fiji image processing package (https://loci.wisc.edu/software/fiji); data is expressed as average lipid droplet size (μm^2). 3) pgWAT adipocyte size assay: 3–6 images across the length of the fat pad were scored for adipocyte size (measured as number of adipocytes/area scored) in each of 4–6 mice (total adipocytes scored >1500/mouse).

Ki67 staining

The mitotic index of skins was determined using the Ventana Discovery UltraBiomarker automated staining instrument, as prescribed by the manufacturer, using the following antibodies: Abcam cat#ab16777 (0.3 μgs/slide) and HRP-conjugated anti-rabbit antibody (Ventana#760-4311). Slides were counterstained with eosin (0.3% in ethanol; Polysciences cat#02740).

Radiotracer administration, assay and skin dissociation

Mice were acclimated to thermoneutrality before administration of Triolein [9,10-3H(N)] (ARC cat#0199), diluted 1:10 in canola oil. Mice were administered 10 μCi /100 μl by gavage, and rehoused into controlled temperature housing, as indicated. Mice were euthanized and tissues dissolved in Solvable (Perkin Elmer cat#6NE9100) according to the manufacturer's instructions, diluted into UltimaGold for liquid scintillation counting. Hair samples were collected for sebome analysis. For the preparation of separated skin fractions, skins were floated dermis side down onto cold elastase/DMEM/Hepes in a 6-well tissue culture dish for 6 h. Tissue dissociation grade elastase (Sigma cat#E1250) was diluted to 0.12 mg/ml into DMEM (Gibco, high glucose cat#11965118) / 20 mM Hepes pH 7.4. Skins were rinsed in PBS, blotted, turned epidermis down and the dWAT layer scraped off manually with forceps. Purity of fractions was established by histology (Supplementary Fig. 10).

Administration of lipoprotein lipase inhibitor, tetrahydrolipstatin (THL)

THL (Orlistat; Sigma cat# 04139)[64] was dissolved in DMSO to 12.5 mg/ml, and diluted 10x prior to use in warm PBS. Drug was administered at 10 μg/g BWt by intraperitoneal injection, 1 hour prior to ^{3}H triolein gavage, following the method of Bartelt et al.[14].

Thin layer chromatography (TLC)

Lipids were extracted from hair (up to 50 mg) sequentially, using firstly 2:1 chloroform: methanol, and then acetone (4 mls each). Extracts were inverted to mix, incubated at room temperature, the extract decanted,

combined and dried down. Lipids were resuspended in 4:1 chloroform:methanol, and loaded onto preparative TLC plates (Supelco TLC silica gel-60 glass plates; Millipore Sigma cat#1.00390.0001), and separated through 3 phases (as described by Choa et al[51]). The first phase was 80:20:1 hexane:isopropyl diether:acetic acid, to 50% plate height, second phase was 1:1 hexane:benzene to 80% plate height, and third phase was hexane, to 90% height. Lipids were visualized either using primuline (0.005% in 80:20 acetone:water)[14] or charring with cupric sulfate (sprayed with 10% cupric sulfate in 8% phosphoric acid, dried, and baked at 300 °F for 10 minutes).

LC/QTOF-MS mass spectrometric analysis of lipids in tissues and sera
Lipidomic analysis was performed according to Simcox et al.[65,66]; briefly, 40 μl aliquots of sera were combined with 250 μls PBS and 225 μls ice-cold MeOH containing internal standards (Avanti Splash cat#3307-07), and homogenized. Samples were then mixed with 750 μls of ice-cold MTBE (methyl tert-butyl ether), re-homogenized, and separated by centrifugation (17,000 g for 5 mins/4 °C). The upper phase was transferred to a new tube, lyophilized and resuspended in 150 μls of isopropanol. Lipids were analyzed by UHPLC/MS/MS in positive and negative ion modes, at a dilution suitable to eliminate saturation issues. Extracts were separated on an Agilent 1260 Infinity II UHPLC system using an Acquity BEH C18 column (Waters 186009453; 1.7 μm 2.1 × 100 mm) maintained at 50 C with VanGuard BEH C18 pre-column (Waters 18003975), using the chromatography gradients described by Jain et al. The UHPLC system was connected to an Agilent 6546 Q-TOF MS dual AJS ESI mass spectrometer and run in both positive and negative modes as described. Samples were injected in a random order and scanned between 100 and 1500 m/z. Tandem MS was performed at a fixed collision energy of 25 V. The injection volume was 2 μl for positive mode and 5 μl for negative mode.

Lipidomic data processing. Methods for data processing were described by Jain et al.[66]. Briefly, MS/MS data were analyzed using Agilent MassHunter Qualitative Analysis and LipidAnnotator for lipid identification[67]. Accuracy of retention times was checked by reference to internal standards. Data was imported into Agilent Profinder for lipid identification and peak integration (using sera-specific libraries). Data were analyzed using MetaboAnalyst free-ware (https://www.metaboanalyst.ca), Microsoft Excel and GraphPad Prism8 software (https://www.graphpad.com/scientific-software/prism).

A reporting overview is provided as Supplemental Data S1. This includes a description of the total inventory screened (tab *total lipid number epi sebome*), and the inventory reported in Figures. The key to the data files provided in the massIVE repository is provided, together with excel files supplemented with diagnostic ion species for each lipid, for each of 8 data sets in positive and negative acquisition mode, for serum, sebome, epidermis and dWAT.

Fatty acid methyl ester (FAME) analysis
Lipids were scraped from TLC plates of separated lipids from 3 mice, and all analyses were performed in duplicate. Lipids were dissolved in toluene (100 μl) and processed to fatty acid methyl esters by base-catalysed transesterification (Lipidmaps.org). Thus, 200 μl of sodium methoxide (FisherSci cat#AC427228000) was added, incubated at 50 °C for 10 min, cooled and acidified with 10 μl acetic acid. To the mixture, 0.5 ml of water were added and vortexed, followed by 0.5ml hexane, vortexing and centrifugation to focus the interface. The top layer was removed, the hexane extraction repeated, and both supernatants pooled and dried down. Products of FAME reactions were evaluated by analytical TLC, run as for preparative TLC runs above, but using a hexane: diethyl ether: acetic acid (8:2:2) solvent run out for 10 cm, followed by charring with cupric sulfate. The FAME mixture was dissolved in anhydrous dicloloromethane, spiked with a C17 FAME

standard (Cayman# 26723) and analyzed by GC/MS on an Agilent 7890B GC coupled to an Agilent 5977 A MSD, with an Agilent DB-23 column (60 m long, 0.25 mm i.d., 0.25 μm film thickness), with a staged injection protocol run at 250 °C. Separating resolution, species identification and reproducibility were assessed using a Supelco 37-FAME standard (cat # CRM47885), and retention times (RTs) were compared to skin sample preparations.

Statistics and reproducibility
The number of independent samples is indicated in the legend to each Figure. Unless otherwise stated, each data point is derived as an average from a single mouse. Data are presented as mean values +/− SD. Unless otherwise stated, p-values are derived from 2-sided t tests, and indicated on Figures as follows: $*p < 0.05$; $**p < 0.01$, $***p < 0.001$, $****p < 0.0001$. The exact p-values are stated in Source Data files.

Reporting summary
Further information on research design is available in the Nature Portfolio Reporting Summary linked to this article.

Data availability
The data supporting the findings from this study are available within the manuscript and its supplementary information. Lipidomic data is deposited at massIVE.ucsd.edu; submission# MSV000094882. The key, together with processed lipidomic data, are provided in Supplementary Data 1. Source Data are provided with this paper Source data are provided with this paper.

References
1. Radner, F. P., Grond, S., Haemmerle, G., Lass, A. & Zechner, R. Fat in the skin: Triacylglycerol metabolism in keratinocytes and its role in the development of neutral lipid storage disease. *Dermatoendocrinol* **3**, 77–83 (2011).
2. Kruse, V., Neess, D. & Faergeman, N. J. The Significance of Epidermal Lipid Metabolism in Whole-Body Physiology. *Trends Endocrinol. Metab.* **28**, 669–683 (2017).
3. Neess, D. et al. Epidermal Acyl-CoA-binding protein is indispensable for systemic energy homeostasis. *Mol. Metab.* **44**, 101144 (2021).
4. Neess, D. et al. Delayed hepatic adaptation to weaning in ACBP-/- mice is caused by disruption of the epidermal barrier. *Cell Rep.* **5**, 1403–1412 (2013).
5. Alexander, C. M. et al. Dermal white adipose tissue: a new component of the thermogenic response. *J. Lipid Res* **56**, 2061–2069 (2015).
6. Kasza, I. et al. Evaporative cooling provides a major metabolic energy sink. *Mol. Metab.* **27**, 47–61 (2019).
7. Sampath, H. & Ntambi, J. M. Role of stearoyl-CoA desaturase-1 in skin integrity and whole body energy balance. *J. Biol. Chem.* **289**, 2482–2488 (2014).
8. Butera, A. et al. ZFP750 affects the cutaneous barrier through regulating lipid metabolism. *Sci. Adv.* **9**, eadg5423 (2023).
9. Liakath-Ali, K. et al. Alkaline ceramidase 1 is essential for mammalian skin homeostasis and regulating whole-body energy expenditure. *J. Pathol.* **239**, 374–383 (2016).
10. Yu, Z. et al. Thermal facial image analyses reveal quantitative hallmarks of aging and metabolic diseases. *Cell Metab.* **36**, 1482–1493.e1487 (2024).
11. Zhang, Q., Sun, Y. & Yang, J. Bio-heat response of skin tissue based on three-phase-lag model. *Sci. Rep.* **10**, 16421 (2020).
12. Zhang, Z. et al. Dermal adipose tissue has high plasticity and undergoes reversible dedifferentiation in mice. *J. Clin. Invest* **129**, 5327–5342 (2019).
13. Marsh, D. Structural and thermodynamic determinants of chain-melting transition temperatures for phospholipid and glycolipids membranes. *Biochim Biophys. Acta* **1798**, 40–51 (2010).

14. Bartelt, A. et al. Brown adipose tissue activity controls triglyceride clearance. *Nat. Med.* **17**, 200–205 (2011).

15. Cummings, N. E. et al. Restoration of metabolic health by decreased consumption of branched-chain amino acids. *J. Physiol.* **596**, 623–645 (2018).

16. Fontana, L. et al. Decreased Consumption of Branched-Chain Amino Acids Improves Metabolic Health. *Cell Rep.* **16**, 520–530 (2016).

17. Ferraz-Bannitz, R. et al. Dietary Protein Restriction Improves Metabolic Dysfunction in Patients with Metabolic Syndrome in a Randomized, Controlled Trial. *Nutrients* **14**, https://doi.org/10.3390/nu14132670 (2022).

18. Yu, D. et al. The adverse metabolic effects of branched-chain amino acids are mediated by isoleucine and valine. *Cell Metab.* **33**, 905–922.e906 (2021).

19. Rabionet, M., Gorgas, K. & Sandhoff, R. Ceramide synthesis in the epidermis. *Biochim Biophys. Acta* **1841**, 422–434 (2014).

20. Chaurasia, B. & Summers, S. A. Ceramides in Metabolism: Key Lipotoxic Players. *Annu Rev. Physiol.* **83**, 303–330 (2021).

21. Kawana, M., Miyamoto, M., Ohno, Y. & Kihara, A. Comparative profiling and comprehensive quantification of stratum corneum ceramides in humans and mice by LC/MS/MS. *J. Lipid Res* **61**, 884–895 (2020).

22. Uche, L. E., Gooris, G. S., Bouwstra, J. A. & Beddoes, C. M. Barrier Capability of Skin Lipid Models: Effect of Ceramides and Free Fatty Acid Composition. *Langmuir* **35**, 15376–15388 (2019).

23. Summers, S. A., Chaurasia, B. & Holland, W. L. Metabolic Messengers: ceramides. *Nat. Metab.* **1**, 1051–1058 (2019).

24. Albeituni, S. & Stiban, J. Roles of Ceramides and Other Sphingolipids in Immune Cell Function and Inflammation. *Adv. Exp. Med Biol.* **1161**, 169–191 (2019).

25. Coderch, L., Lopez, O., de la Maza, A. & Parra, J. L. Ceramides and skin function. *Am. J. Clin. Dermatol* **4**, 107–129 (2003).

26. Radner, F. P. & Fischer, J. The important role of epidermal triacylglycerol metabolism for maintenance of the skin permeability barrier function. *Biochim Biophys. Acta* **1841**, 409–415 (2014).

27. van Smeden, J. & Bouwstra, J. A. Stratum Corneum Lipids: Their Role for the Skin Barrier Function in Healthy Subjects and Atopic Dermatitis Patients. *Curr. Probl. Dermatol* **49**, 8–26 (2016).

28. Plikus, M. V. & Chuong, C. M. Complex hair cycle domain patterns and regenerative hair waves in living rodents. *J. investigative Dermatol.* **128**, 1071–1080 (2008).

29. Shook, B. A. et al. Dermal Adipocyte Lipolysis and Myofibroblast Conversion Are Required for Efficient Skin Repair. *Cell Stem Cell* **26**, 880–895.e886 (2020).

30. Zhang, Z. et al. Dermal adipocytes contribute to the metabolic regulation of dermal fibroblasts. *Exp. Dermatol* **30**, 102–111 (2021).

31. Forni, M. F. et al. Caloric Restriction Promotes Structural and Metabolic Changes in the Skin. *Cell Rep.* **20**, 2678–2692 (2017).

32. Hunt, N. D. et al. Effect of calorie restriction and refeeding on skin wound healing in the rat. *Age (Dordr.)* **34**, 1453–1458 (2012).

33. Cai, J. et al. The browning and mobilization of subcutaneous white adipose tissue supports efficient skin repair. *Cell Metab.* **36**, 1287–1301.e1287 (2024).

34. Schmidt, B. A. & Horsley, V. Intradermal adipocytes mediate fibroblast recruitment during skin wound healing. *Development* **140**, 1517–1527 (2013).

35. Chen, H. et al. Intermittent fasting triggers interorgan communication to suppress hair follicle regeneration. *Cell* **188**, 157–174.e122 (2025).

36. Triwatcharikorn, J. et al. Skin manifestations and biophysical changes following weight reduction induced by bariatric surgery: A 2-year prospective study. *J. Dermatol* **50**, 1635–1639 (2023).

37. Chen, V. Y., Siegfried, L. G., Tomic-Canic, M., Stone, R. C. & Pastar, I. Cutaneous changes in diabetic patients: Primed for aberrant healing? *Wound Repair Regen.* **31**, 700–712 (2023).

38. Felix, J. B., Cox, A. R. & Hartig, S. M. Acetyl-CoA and Metabolite Fluxes Regulate White Adipose Tissue Expansion. *Trends Endocrinol. Metab.* **32**, 320–332 (2021).

39. Wu, S. A., Kersten, S. & Qi, L. Lipoprotein Lipase and Its Regulators: An Unfolding Story. *Trends Endocrinol. Metab.* **32**, 48–61 (2021).

40. Nguyen, P. T. T. et al. Acetyl-CoA synthesis in the skin is a key determinant of systemic lipid homeostasis. *Cell Rep.* **44**, 115284 (2025).

41. O'Neill, C. A., Monteleone, G., McLaughlin, J. T. & Paus, R. The gut-skin axis in health and disease: A paradigm with therapeutic implications. *Bioessays* **38**, 1167–1176 (2016).

42. Xiao, X. et al. The role of short-chain fatty acids in inflammatory skin diseases. *Front Microbiol* **13**, 1083432 (2022).

43. Cros, A. et al. Homeostatic activation of aryl hydrocarbon receptor by dietary ligands dampens cutaneous allergic responses by controlling Langerhans cells migration. *elife* **12**, e86413 (2023).

44. Kasza, I. et al. Contrasting recruitment of skin-associated adipose depots during cold challenge of mouse and human. *J. Physiol.* https://doi.org/10.1113/JP280922 (2021).

45. Morigny, P., Boucher, J., Arner, P. & Langin, D. Lipid and glucose metabolism in white adipocytes: pathways, dysfunction and therapeutics. *Nat. Rev. Endocrinol.* **17**, 276–295 (2021).

46. Arner, P. & Ryden, M. Human white adipose tissue: A highly dynamic metabolic organ. *J. Intern Med* **291**, 611–621 (2022).

47. Kasza, I. et al. Syndecan-1 is required to maintain intradermal fat and prevent cold stress. *PLoS Genet* **10**, e1004514 (2014).

48. Plikus, M. V. et al. Cyclic dermal BMP signalling regulates stem cell activation during hair regeneration. *Nature* **451**, 340–344 (2008).

49. Zouboulis, C. C., Yoshida, G. J., Wu, Y., Xia, L. & Schneider, M. R. Sebaceous gland: Milestones of 30-year modelling research dedicated to the "brain of the skin. *Exp. Dermatol* **29**, 1069–1079 (2020).

50. Zouboulis, C. C. et al. Sebaceous immunobiology - skin homeostasis, pathophysiology, coordination of innate immunity and inflammatory response and disease associations. *Front Immunol.* **13**, 1029818 (2022).

51. Choa, R. et al. Thymic stromal lymphopoietin induces adipose loss through sebum hypersecretion. *Science* **373**, https://doi.org/10.1126/science.abd2893 (2021).

52. Almoughrabie, S. et al. Commensal Cutibacterium acnes induce epidermal lipid synthesis important for skin barrier function. *Sci. Adv.* **9**, eadg6262 (2023).

53. Christ, A. et al. Western Diet Triggers NLRP3-Dependent Innate Immune Reprogramming. *Cell* **172**, 162–175.e114 (2018).

54. Herbert, D. et al. High-Fat Diet Exacerbates Early Psoriatic Skin Inflammation Independent of Obesity: Saturated Fatty Acids as Key Players. *J. Invest Dermatol* **138**, 1999–2009 (2018).

55. Higashi, Y. et al. High-fat diet exacerbates imiquimod-induced psoriasis-like dermatitis in mice. *Exp. Dermatol* **27**, 178–184 (2018).

56. Shi, Z. et al. Short-Term Western Diet Intake Promotes IL-23–Mediated Skin and Joint Inflammation Accompanied by Changes to the Gut Microbiota in Mice. *J. Invest Dermatol* **141**, 1780–1791 (2021).

57. Yu, S. et al. A Western Diet, but Not a High-Fat and Low-Sugar Diet, Predisposes Mice to Enhanced Susceptibility to Imiquimod-Induced Psoriasiform Dermatitis. *J. Invest Dermatol* **139**, 1404–1407 (2019).

58. Hao, J. et al. Consumption of fish oil high-fat diet induces murine hair loss via epidermal fatty acid binding protein in skin macrophages. *Cell Rep.* **41**, 111804 (2022).

59. Kleiboeker, B. & Lodhi, I. J. Peroxisomal regulation of energy homeostasis: Effect on obesity and related metabolic disorders. *Mol. Metab.* **65**, 101577 (2022).

60. Nakamura, M. T., Yudell, B. E. & Loor, J. J. Regulation of energy metabolism by long-chain fatty acids. *Prog. Lipid Res* **53**, 124–144 (2014).

61. McCoin, C. S., Knotts, T. A. & Adams, S. H. Acylcarnitines-old actors auditioning for new roles in metabolic physiology. *Nat. Rev. Endocrinol.* **11**, 617–625 (2015).

62. Li, Z. et al. Lipolysis of bone marrow adipocytes is required to fuel bone and the marrow niche during energy deficits. *elife* **11** https://doi.org/10.7554/eLife.78496 (2022).

63. Kasza, I. et al. Humanizing" mouse environments: Humidity, diurnal cycles and thermoneutrality. *Biochimie* **210**, 82–98 (2023).

64. Augustus, A. S., Kako, Y., Yagyu, H. & Goldberg, I. J. Routes of FA delivery to cardiac muscle: modulation of lipoprotein lipolysis alters uptake of TG-derived FA. *Am. J. Physiol. Endocrinol. Metab.* **284**, E331–339 (2003).

65. Simcox, J. et al. Global Analysis of Plasma Lipids Identifies Liver-Derived Acylcarnitines as a Fuel Source for Brown Fat Thermogenesis. *Cell Metab.* **26**, 509–522.e506 (2017).

66. Jain, R., Wade, G., Ong, I., Chaurasia, B. & Simcox, J. Determination of tissue contributions to the circulating lipid pool in cold exposure via systematic assessment of lipid profiles. *J. Lipid Res* **63**, 100197 (2022).

67. Horing, M. et al. Accurate quantification of lipid species affected by isobaric overlap in Fourier-transform mass spectrometry. *J. Lipid Res* **62**, 100050 (2021).

Acknowledgements

Author contributions

Conceptualization, methodology: C.M.A., D.W.L., R.J., J.A.S.; Experimental procedures: N.R., I.K., I.D.K.H., M.E.T., G.B.-W., R.J., C.M.A.; Resources: C.-L.E.Y., J.A.S.; Writing, editing: C.M.A., O.A.M., D.W.L.

Competing interests

The authors declare no competing interests.

Additional information